Aalborg Universitet

Internal Model Control for AUVs with Output Time Delays and Input Disturbances

Pedersen, Simon; Liniger, Jesper; Sørensen, Fredrik Fogh; von Benzon, Malte; Nielsen, Morten Eggert; Mai, Christian

Link to publication from Aalborg University

Internal Model Control for AUVs with Output Time Delays and Input Disturbances

Simon Pedersen [**], **Jesper Liniger**, **Fredrik Fogh Sørensen**,
Malte von Benzon, **Morten Eggert Nielsen**, **Christian Mai**

AAU Energy, Aalborg University, Niels Bohrs Vej 8, DK-6700 Esbjerg, Denmark
** *Corresponding author. E-mail: spe@energy.aau.dk.*

Abstract: Autonomous Underwater Vehicles (AUVs) are increasingly being used for offshore inspection tasks. This paper investigates how navigation using Simple Internal Model Control for Proportional-Integral-Derivative Control (SIMC-PID) operates in a realistic offshore environment with waves and ocean current acting as input disturbances while the available underwater sensors introduce time delays on the output signals. First, the time delays are determined by investigating available absolute positioning sensor systems. Then, a model of the AUV and the external disturbances is established. The model-based SIMC-PID controller is tuned and examined based on acceptable disturbance rejection while tolerating the dominant time delays. Two simulation case studies show that the heave controller, in both cases, struggles to stabilize in 0 to 8 meters depths, while the surge and sway controllers tolerate the Doppler Velocity Log case (DVL) acceptably. Short Baseline (SBL) shows unacceptable performance in 0 to 15 meters depths. It is concluded that the simplicity of the SIMC-PID controller is an advantage and, therefore, useful when time delays are relatively small, but more advanced techniques must be applied for larger delays such as those introduced by SBL systems.

Keywords: IMC, AUV, Underwater Robotics, Time Delay, Offshore, Disturbance Rejection

1. INTRODUCTION

Over the last decade, there has been an increasing demand for Unmanned Underwater Vehicles (UUVs) for operations, such as seabed mapping, harbor monitoring, offshore maintenance, and surveillance of critical infrastructure (Mai et al. (2016)). Remotely operated vehicles (ROVs) and autonomous underwater vehicle (AUVs) has increased value for the offshore industry as the expenses used on ROV and AUV operations have increased during the last decade while the offshore industry itself has expanded and still will in the future (Brun (2012)). Therefore, automating the operation done by the ROVs and AUVs will be increasingly beneficial as well (Tena (2011)). Some energy-costly operations demand a tethered ROV due to the limited battery lifetime of AUVs (Pedersen et al. (2022)), however, several operations, such as inspections, are typically carried out by light AUVs due to the maneuverability and mobility (Liniger et al. (2022)).

One important requirement for completing such AUV operations is accurate localization (Yang and Huang (2017); Paull et al. (2014)). Several common localization sensors developed for underwater navigation induce dominant measurement output time delays weakening the possibility for feedback control applications (Pedersen et al. (2019)). Besides the output time delays, operations in offshore environments include various external disturbances, such as waves and underwater ocean current. Both the output time delays and external disturbances problematise the AUV

efficiency, especially at near-structure operations where precision is more demanding than in open water, where the allowed navigation error is larger.

This study will investigate the development of a decentralized Simple Internal Model Control (SIMC-PID) scheme where the output delays are explicitly included in the PID coefficients, as described in Skogestad (2003); Skogestad and Grimholt (2012). Thus, the main advantage of using the SIMC-PID scheme is the simple tuning procedure. Realistic time delays have been determined based on typical underwater positioning sensors; Short Baselines (SBL) and Doppler Velocity Logs (DVL) and the work in Skogestad (2006) demonstrated the SIMC-PID provided decent disturbance rejection and, hence, this study will examine how well the developed controller rejects offshore disturbances from waves and underwater ocean currents. The simulation results will be based on verified AUV, wave and current models, combined into a single model. Lastly, a conclusion and future work will be presented.

2. SUBSEA SENSOR-INDUCED TIME DELAY

Real-time underwater positioning for autonomous navigation is challenging as common sensor technologies, such as Global Positioning System (GPS) signals, do not penetrate water (Paull et al. (2014)). Thus, efforts have been put into developing sensors dedicated to underwater applications. Acoustic sensor technologies have shown potential for underwater navigation, where SBL and DVL are com-

Tab. 1. Acoustic sensor technologies for underwater positioning.

Sensor	Sources	Sensor Delay	Range	Pros	Cons
SBL	Kebkal and Mashoshin (2017); Pedersen et al. (2019)	~2s	Up to 100 m	Accuracy	Demands externally fixed transponders
DVL	Snyder (2010); Karmozdi et al. (2018)	0.2 s	18–100 m	Onboard	Accumulating error through integration

monly applied in narrow range applications; see Tab. 1. It must be noted that SBLs can be replaced by Long Baseline (LBL) and Ultrashort Baseline (USBL) systems, but LBLs demand impractical sea-floor mounted baseline transponders and USBLs has limited line of sight coverage due to the reduced transducer spacing (Vickery (1998)). Moreover, several underwater relative positioning sensors exist, but they all demand an object for distance estimation, which is not available when navigating in open water e.g. between subsea structures. As seabeds are easier to identify, the DVLs provide more consistent measurement signals. Therefore, in this study, two cases are considered; (1) a DVL sensor with 0.2 seconds time delay, and (2) an SBL sensor with 2 seconds time delay. The delays are introduced for the linear motions in two of the space dimensions; N and E illustrated in Fig. 1. For the remaining motion measurements, 0.1 seconds time delay is implemented to represent the time delay from communication transmission, computational time, and noise filtering for an Inertial measurement unit (IMU) with a magnetometer and pressure transmitter.

3. AUV MODELING

The modeling of the AUV is based on Fossen representation for underwater vehicles Fossen (2011), and the parameters have been determined through a combination of experiments. The details on the parameters and actuation can be found in Benzon et al. (2022). Please notice that some of the parameters in Tab. 3 have been modified to improve model accuracy. The governing equations are given by.

$$\dot{\boldsymbol{\eta}} = \boldsymbol{J}(\boldsymbol{\eta})\boldsymbol{\nu} \tag{1}$$

$$\boldsymbol{M}\dot{\boldsymbol{\nu}} + \boldsymbol{C}(\boldsymbol{\nu})\boldsymbol{\nu} + \boldsymbol{D}(\boldsymbol{\nu})\boldsymbol{\nu} + \boldsymbol{g}(\boldsymbol{\eta}) = \bar{\boldsymbol{\tau}} \tag{2}$$

where $\boldsymbol{\eta} = \left[N, E, D, \bar{\phi}, \bar{\theta}, \psi \right]^T$ is a combination of world coordinates and Euler angles defined in the NED frame. $\boldsymbol{\nu} = [u, v, w, p, q, r]^T$ is the body-fixed velocity vector. In Fig. 1 both the NED and body-fixed frame definitions are shown.
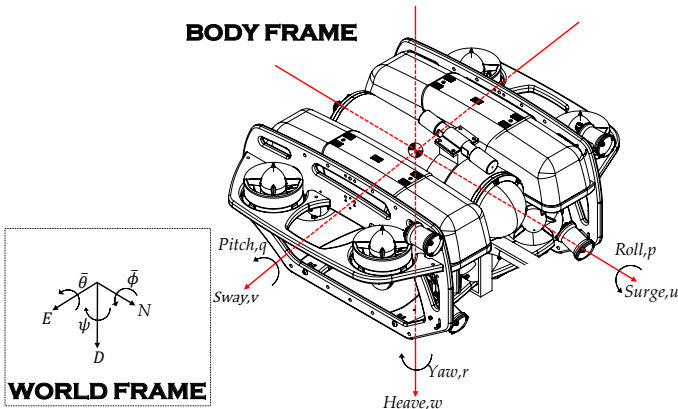

Fig. 1. Figure from Benzon et al. (2021). BlueROV2 with frame-definitions in both body and world frame, respectively.

$J(\eta)$ is the rotation matrix. For the external forces $\bar{\boldsymbol{\tau}} = \left[\tau_x, \tau_y, \tau_z, \tau_{\bar{\phi}}, \tau_{\bar{\theta}}, \tau_\psi \right]^T$, which is the input given in force and torque The rest of the variables in Eq. (1) and Eq. (2) can be seen in Tab. 2.

Tab. 2. Variables and their components.

Notation	Components
$\boldsymbol{M}$	$\boldsymbol{M}_{rb} + \boldsymbol{M}_a$
$\boldsymbol{M}_{rb}$	$\mathrm{diag}(m, m, m, I_x, I_y, I_z)$
$\boldsymbol{M}_a$	$-\mathrm{diag}(X_{\dot{u}}, Y_{\dot{v}}, Z_{\dot{w}}, K_{\dot{p}}, M_{\dot{q}}, N_{\dot{r}})$
$\boldsymbol{C}(\boldsymbol{\nu})$	$\begin{bmatrix} \boldsymbol{0} & \boldsymbol{C}_1(\nu) \\ \boldsymbol{C}_1(\nu) & \boldsymbol{C}_2(\nu) \end{bmatrix}$
$\boldsymbol{C}_1(\boldsymbol{\nu})$	$\begin{bmatrix} 0 & (m - Z_{\dot{w}})w & (Y_{\dot{v}} - m)v \\ (Z_{\dot{w}} - m)w & 0 & (m - X_{\dot{u}})u \\ (m - Y_{\dot{v}})v & (X_{\dot{u}} - m)u & 0 \end{bmatrix}$
$\boldsymbol{C}_2(\boldsymbol{\nu})$	$\begin{bmatrix} 0 & -(I_z + N_{\dot{r}})r & (M_{\dot{q}} - I_y)q \\ (N_{\dot{r}} + I_z)r & 0 & (I_x - K_{\dot{p}})p \\ (I_y - M_{\dot{q}})q & (K_{\dot{p}} - I_x)p & 0 \end{bmatrix}$
$\boldsymbol{D}(\boldsymbol{\nu})$	$-\mathrm{diag}(X_u(u), Y_v(v), Z_w(w), K_p(p), M_q(q), N_r(r))$
$\boldsymbol{g}(\boldsymbol{\eta})$	$\begin{bmatrix} (W - B)\sin(\bar{\theta}) \\ -(W - B)\cos(\bar{\theta})\sin(\bar{\phi}) \\ -(W - B)\cos(\bar{\theta})\cos(\bar{\phi}) \\ y_b B\cos(\bar{\theta})\cos(\bar{\phi}) - z_b B\cos(\bar{\theta})\sin(\bar{\phi}) \\ -z_b B\sin(\bar{\theta}) - x_b B\cos(\bar{\theta})\cos(\bar{\phi}) \\ x_b B\cos(\bar{\theta})\sin(\bar{\phi}) + y_b B\sin(\bar{\theta}) \end{bmatrix}$
W	mg
B	$\rho g \nabla$

Tab. 3. Parameters used for the model. Modified parameters indicated by *.

Notation	Values/Term	Unit
g	9.82	$\mathrm{m\,s^{-2}}$
ρ	1000	$\mathrm{kg\,m^{-3}}$
m	13.5	kg
∇	0.0133	$\mathrm{m^3}$
(I_x, I_y, I_z)	(0.26, 0.23, 0.37)	$\mathrm{kg\,m^2}$
(x_b, y_b, z_b)	(0, 0, -0.01)	m
$X_{\dot{u}}$	6.36	kg
$Y_{\dot{v}}$	7.12	kg
$Z_{\dot{w}}$	18.68	kg
$K_{\dot{p}}$	0.189	$\mathrm{kg\,m^2}$
$M_{\dot{q}}$	0.135	$\mathrm{kg\,m^2}$
$N_{\dot{r}}$	0.222	$\mathrm{kg\,m^2}$
$X_u(u)$	$141|u| + 13.7$	$\mathrm{N\,s\,m^{-1}}$
$Y_v(v)$	$184.3|v| + 20$*	$\mathrm{N\,s\,m^{-1}}$
$Z_w(w)$	$190|w| + 33$	$\mathrm{N\,s\,m^{-1}}$
$K_p(p)$	$0.95|p| + 0.15$*	$\mathrm{N\,s}$
$M_q(q)$	$0.47|q| + 0.8$	$\mathrm{N\,s}$
$N_r(r)$	$1.17|r| + 0.2$*	$\mathrm{N\,s}$

To get a mathematical expression for the acceleration equation Eq. (2) is solved as an inverse problem with respect to $\dot{\boldsymbol{\nu}}$.

$$\dot{\boldsymbol{\nu}} = \boldsymbol{M}^{-1}\left(\bar{\boldsymbol{\tau}} - \boldsymbol{C}(\boldsymbol{\nu})\boldsymbol{\nu} - \boldsymbol{D}(\boldsymbol{\nu})\boldsymbol{\nu} - \boldsymbol{g}(\boldsymbol{\eta})\right) \tag{3}$$

This can then be formulated as a vector of nonlinear functions.

$$\boldsymbol{f}(\boldsymbol{\eta}, \boldsymbol{\nu}, \bar{\boldsymbol{\tau}}) = [\dot{u}(\boldsymbol{\eta}, \boldsymbol{\nu}, \bar{\boldsymbol{\tau}}), \dot{v}(\boldsymbol{\eta}, \boldsymbol{\nu}, \bar{\boldsymbol{\tau}}), \dot{w}(\boldsymbol{\eta}, \boldsymbol{\nu}, \bar{\boldsymbol{\tau}}),$$
$$\dot{p}(\boldsymbol{\eta}, \boldsymbol{\nu}, \bar{\boldsymbol{\tau}}), \dot{q}(\boldsymbol{\eta}, \boldsymbol{\nu}, \bar{\boldsymbol{\tau}}), \dot{r}(\boldsymbol{\eta}, \boldsymbol{\nu}, \bar{\boldsymbol{\tau}})]^T \tag{4}$$

From Eq. (3) and Tab. 2 it can noted that the non-linear model only depends on $\bar{\phi}$ and $\bar{\theta}$ from η. Both are set to zero due to restoring forces. Therefore, $\boldsymbol{f}(\boldsymbol{\eta}, \boldsymbol{\nu}, \bar{\boldsymbol{\tau}})$ becomes $\boldsymbol{f}(\boldsymbol{\nu}, \bar{\boldsymbol{\tau}})$, where $\boldsymbol{\nu}$ is the state matrix and $\bar{\boldsymbol{\tau}}$ is the input matrix.

4. MODELING OF EXTERNAL DISTURBANCES

The main disturbances in an offshore environment can considered to be water waves and underwater current. In this section, we will briefly outline how these disturbances are modeled.

4.1 Ocean waves

Tab. 4. Definitions of wave variables.

Notation	Description
a	Wave amplitude
c	Spreading index
d	Water depth
f	Wave frequency
f_P	Peak wave frequency
H_s	The significant wave height
L	Wavelength
i, j	Index number
k	Wavenumber
n and m	Natural numbers
$S(f,\zeta), S_{JS}(f)$	Water wave spectrum
T_p	Peak wave period
t	Time
$X(\zeta)$	Spreading function
γ	Peak enhancement factor
ζ	Wave direction
Π	Surface elevation
Θ	Angular wave frequency
$\Gamma(n)$	Gamma function
μ	Random phase

The disturbance caused by the wave motion is estimated by a Morison-type equation (Avila and Adamowski (2011); Sayer (2008)) expressed here as

$$\bar{\boldsymbol{\tau}}_w = \boldsymbol{D}_w(\boldsymbol{\nu}_w - \boldsymbol{\nu}_1)|\boldsymbol{\nu}_w - \boldsymbol{\nu}_1| + (\boldsymbol{M}_w\dot{\boldsymbol{\nu}}_w - \boldsymbol{M}_{a,w}\dot{\boldsymbol{\nu}}_1) \quad (5)$$

where $\boldsymbol{\nu}_w = (u_w, v_w, w_w)$ are the fluid particle velocities, $\boldsymbol{D}_w(\boldsymbol{\nu}_w - \boldsymbol{\nu}_1) = \boldsymbol{D}(1{:}3, 1{:}3)$ is the force caused by drag, $\boldsymbol{M}_w = \boldsymbol{M}(1{:}3, 1{:}3)$, $\boldsymbol{M}_{a,w} = \boldsymbol{M}_a(1{:}3, 1{:}3)$ and $\boldsymbol{\nu}_1 = [u, v, w]^T$. The fluid particle velocities are computed from the JONSWAP wave spectrum Hasselmann (1973) with a spreading function which grant multi-directional and irregular water waves. The approach has been used to model waves on a tethered ROV deployed to clean offshore structures in Benzon et al. (2022).

$$S(f, \zeta) = S_{JS}(f) X(\zeta) \quad (6)$$

where S_{JS} is the JONSWAP wave spectrum and $X(\zeta)$ is a spreading function. The JONSWAP spectrum is given by,

$$S_{JS}(f) = C(\gamma)\frac{5}{16}H_s^2\frac{f_P^4}{f^5}e^{\left(-\frac{5f_P^4}{4f^4}\right)}\gamma^{e^{\left(-\frac{(f-f_P)^2}{2(\sigma f_P)^2}\right)}} \quad (7)$$

where $C(\gamma) = 1 - \ln(\gamma)\,0.287$ is a normalizing factor, and σ_w is the spectral width parameter and is 0.07 for $f \leq f_p$ and 0.09 for $f > f_p$.

To model the directional short-crested waves, we introduce a spreading function from DNV (Det Norske Veritas) (2021), which is defined for $|\zeta - \zeta_p| \leq \frac{\pi}{2}$ as

$$X(\zeta) = \frac{\Gamma(1 + \frac{c}{2})}{\sqrt{\pi}\Gamma(0.5 + \frac{c}{2})}cos^c(\zeta - \zeta_p) \quad (8)$$

where Γ is the gamma function and ζ_p is the mean wave direction. Typical values for the spreading index c for wind driven for between 2-4 for a wind-driven sea state (DNV (Det Norske Veritas) (2021)).

By assuming potential flow a model of the surface elevation can be derived of the short-crested sea state by using the principle of superposition, i.e. $n \times m$ linear regular waves are superimposed,

$$\Pi(N, E, t) = \sum_{i=1}^{n}\sum_{j=1}^{m}a_{ij}\cos(\epsilon(N, E, t)_{ij}) \quad (9)$$

where $a_{ij} = \sqrt{2S_{JS}(f_i)X(\zeta_j)\Delta f\Delta\zeta}$ is the amplitude of the ith frequency in the jth direction, where Δf is the frequency bandwidth and $\Delta\zeta$ is the direction bandwidth. To be concise we have defined,

$$\epsilon(N, E, t)_{ij} = \Theta_i t - k_i(N cos(\zeta_j) + E sin(\zeta_j)) + \mu_{ij} \quad (10)$$

where $\Theta_i = 2\pi f_i$ is the angular wave frequency, $k_i = \frac{2\pi}{L_i}$ is the wavenumber, ζ_j is the wave direction and μ_{ij} is the random phase angle for each linear wave component. To realize the free surface, the wavenumbers are required for each wave component and have to be derived by iteration using an different form of the dispersion relation,

$$L_i = \frac{gT_i^2}{2\pi}\tanh\left(\frac{2\pi d}{L_i}\right) \quad (11)$$

where the deep water wavelength $L_i^0 = \frac{gT^2}{2\pi}$ is used as an initial guess for each component.

By assuming potential flow, the fluid particle velocities and accelerations can be obtained from the superimposed velocity potentials related to each wave component,

$$u_w = \sum_{i=1}^{n}\sum_{j=1}^{m}\frac{a_{i,j}gk_i}{\Theta_i}cos(\zeta_j)\Lambda_{ij}^{cosh}\cos(\epsilon_{ij}) \quad (12)$$

$$v_w = \sum_{i=1}^{n}\sum_{j=1}^{m}\frac{a_{i,j}gk_i}{\Theta_i}sin(\zeta_j)\Lambda_{ij}^{cosh}\cos(\epsilon_{ij}) \quad (13)$$

$$w_w = \sum_{i=1}^{n}\sum_{j=1}^{m}-\frac{a_{i,j}gk_i}{\Theta_i}\Lambda_{ij}^{sinh}\sin(\epsilon_{ij}) \quad (14)$$

$$\dot{u}_w \approx \sum_{i=1}^{n}\sum_{j=1}^{m}-a_{i,j}gk_i cos(\zeta_j)\Lambda_{ij}^{cosh}\sin(\epsilon_{ij}) \quad (15)$$

$$\dot{v}_w \approx \sum_{i=1}^{n} \sum_{j=1}^{m} -a_{i,j} g k_i sin(\zeta_j) \Lambda_{ij}^{cosh} \sin(\epsilon_{ij}) \qquad (16)$$

$$\dot{w}_w \approx \sum_{i=1}^{n} \sum_{j=1}^{m} -a_{i,j} g k_i \Lambda_{ij}^{sinh} \cos(\epsilon_{ij}) \qquad (17)$$

where $\epsilon_{ij} = \epsilon(N, E, t)_{ij}$ has been used together with the following definitions

$$\Lambda_{ij}^{sinh} = \Lambda(D)_{ij}^{sinh} = \frac{sinh(k_i(-D+d))}{cosh(k_i d)} \qquad (18)$$

$$\Lambda_{ij}^{cosh} = \Lambda(D)_{ij}^{cosh} = \frac{cosh(k_i(-D+d))}{cosh(k_i d)} \qquad (19)$$

which can now be used in the wave force disturbance vector in Eq. (5).

4.2 Underwater current

The effect of the current is implemented in Eq. (2) as an additional velocity term that is constant in the water column, given by,

$$\boldsymbol{M}\dot{\boldsymbol{\nu}} + \boldsymbol{C}(\boldsymbol{\nu}_r)\boldsymbol{\nu}_r + \boldsymbol{D}(\boldsymbol{\nu}_r)\boldsymbol{\nu}_r + \boldsymbol{g}(\boldsymbol{\eta}) = \bar{\boldsymbol{\tau}} + \bar{\boldsymbol{\tau}}_w \qquad (20)$$

Eq. (20) is in terms of relative velocity in body frame given by $\boldsymbol{\nu}_r = \boldsymbol{\nu} - \boldsymbol{\nu}_c$. The current in world frame is given by $\boldsymbol{v}_c$, the body frame current is specified by,

$$\boldsymbol{\nu}_c = \boldsymbol{R}^{-1} \boldsymbol{v}_c \qquad (21)$$

where,

$$\boldsymbol{v}_c = (u_c, j_c, w_c, 0, 0, 0)^\top \qquad (22)$$

u_c, j_c, w_c is the world frame velocity in north, east and down direction respectably.

5. CONTROLLER DESCRIPTION

SIMC-PID is a systematic procedure for finding the coefficients of a series (cascade) form PID controller:

$$C_{pid}(s) = \frac{U(s)}{E(s)} = K_c \left(\frac{\tau_I s + 1}{\tau_I s} \right)(\tau_D s + 1) \qquad (23)$$

where K_c is the controller gain, τ_I the integral time, and τ_D the derivative time. Compared to alternative tuning rules, SIMC-PID works well for both integrating and pure time delay processes, and for both setpoints and load disturbances; see Skogestad (2003). The main motivation for using SIMC-PID can be summarized to be (Skogestad and Grimholt (2012); Skogestad (2006)):

- The tuning rules are well motivated, model-based and analytically derived. The time delay is explicitly included in the controller coefficients.
- It has shown to work well on a wide range of applications and has demonstrated acceptable disturbance rejection.
- The tuning rules are simple and easy to memorize.

In this study, 0 m/s (for linear velocities) and 0 rad/s (for angular velocities) are used as operational points for linearization, as stable positions are required for most offshore operations.

For $\bar{\phi}$ and $\bar{\theta}$ the respective linearized models can be expressed as second-order transfer functions with left-half

plane (LHP) real-valued poles. Consider a second-order transfer function model, $G(s)$ describing the dynamics of the system:

$$G(s) = \frac{k}{(\tau_1 s + 1)(\tau_2 s + 1)} e^{-\theta s} \qquad (24)$$

where the time delay is rewritten based on Pade's approximation:

$$e^{-\theta s} = 1 - \theta s \qquad (25)$$

then the controller, $C_{pid}(s)$, is

$$C_{pid}(s) = \frac{U(s)}{E(s)} = \frac{(\tau_1 s + 1)(\tau_2 s + 1)}{k(\tau_c + \theta)s} \qquad (26)$$

where τ_c is the sole tuning parameter. This is a cascade form PID controller with

$$K_c = \frac{1}{k}\frac{\tau_1}{\tau_c + \theta}, \ \tau_I = \tau_1, \ \tau_D = \tau_2 \qquad (27)$$

In some cases it is necessary to modify the integral time for improving the disturbance rejection, especially for input disturbances as the wave and current loads introduced in this work. Hence, τ_I is modified such that

$$\tau_I = min\{\tau_1, \ 4(\tau_c + \theta)\} \qquad (28)$$

τ_c can be chosen freely but the optimal value is a trade-off between fast response with good disturbance rejection (favored by a small value of τ_c) and robustness (favored by a large value of τ_c) and in this work is obtained by choosing $\tau_c = \theta$ as recommended in Skogestad (2003). Please notice that $\bar{\phi}$ and $\bar{\theta}$ values yield an underdamped system, which according to Manum (2005) demands rewriting of Eq. (24) and Eq. (26), such that

$$G(s) = \frac{k}{(\tau_0^2 s^2 + 2\tau_0 \phi s + 1)} e^{-\theta s} \qquad (29)$$

where $0 < \phi < 1$ is the damping factor and τ_0 is the time constant, such that $\tau_0 = 1/\omega_n$ where ω_n is the natural frequency. The updated controller, $C_{pid}(s)$, for Eq. (29) is

$$C_{pid}(s) = \frac{1}{k}\frac{1}{k(\tau_c + \theta)s}(\tau_0^2 s^2 + 2\tau_0 \phi s + 1) \qquad (30)$$

For N, E, D, and ψ the respective linearized models can be expressed as second-order type-1 transfer functions with one LHP pole and one pole at the origin. For this, consider a transfer function model, $G_2(s)$, describing the dynamics of the system using an integrator with lag:

$$G_2(s) = \frac{k'}{s(\tau_2 s + 1)} e^{-\theta s} \qquad (31)$$

where $k' := k/\tau_2$. Once again, Pade's approximation in Eq. (25) and the control structure as in Eq. (23) are used, where:

$$K_c = \frac{1}{k'}\frac{1}{\tau_c + \theta}, \ \tau_I = 4(\tau_c + \theta), \ \tau_D = \tau_2 \qquad (32)$$

6. RESULTS

This section examines the results from two offshore cases, where the time delay (θ) values are 0.2 and 2 seconds, respectively, as discussed in section 2. In both cases, the references are set to zero for all positions except for the D direction, where the reference is changed with a series of steps from the initial position at 25 meters depth to the splash zone (defined as the range between 0-5 meters depths) at 3 meters depths. As the AUV approaches

the sea surface the wave-induced disturbance will be increasing. Then, it will be investigated how close the AUV can go to the sea surface before reaching instability.

The operating conditions for the ocean waves and current will be based on data collected from an offshore structure located in the North sea. The parameters for wave and current are shown in Tab. 5, note that ocean current is from east.

Tab. 5. Wave and current constants.

Notation	Value	Units
c	2	-
d	50	m
H_s	1	m
T_p	5	sec
u_c, w_c	0	ms^{-1}
j_c	0.1	ms^{-1}
γ	3.3	-
ζ	-0.7854	rad

6.1 Case study: DVL ($\theta = 0.2$)

The results are evaluated based on input actuation and output response at each respective step. It is clear that the closer the AUV is to the sea surface ($D = 0$) the more force is demanded from the thrusters. Figure 2 shows the depth variations from the reference value and the ROV approaches the sea level (from 8 to 4 meters). At larger depths the fluctuations are neglectable, but the figure clearly shows the disturbance effects are difficult to reject for the controller when the operating range is above 8 meters. The roll, pitch, and yaw motions have not been plotted as the induced oscillations are small relative to the linear motion's oscillations and therefore they are being evaluated as providing acceptable performances.
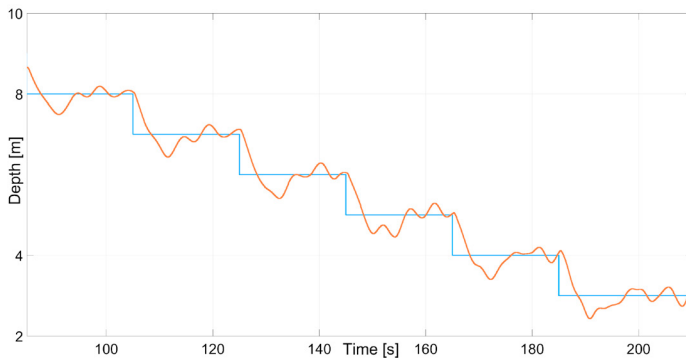

Fig. 2. For $\theta = 0.2$: The depth reference (blue) in the range from 8 to 4 meters compared to the measured value (red).

Fig. 3 shows the entire range for N and E where the references are 0. The AUV is gradually oscillating more as the depth decreases. At around 5 meters depth the AUV oscillates with $\pm$ 0.2 meters which is typically too much for inspection tasks. Therefore, the results show that the SIMC-PID controller tolerates the given disturbances acceptably until around 7 meters depth.
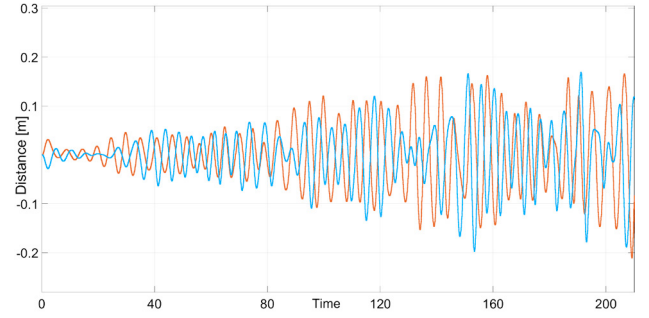

Fig. 3. For $\theta = 0.2$: The N (red) and E (blue) measured values where the references are 0, but the AUV is heaving step-wise.

6.2 Case study: SBL ($\theta = 2$)

In comparison to the DVL the N and E directions' time delays have been changed from 0.2 to 2 seconds which means these are the motions of interest. Both motions have larger oscillations at varying frequencies as can be seen in Fig. 4. The results are summarized in Tab. 6 where the two cases are compared. It is clear that the controller struggle to reject the disturbances especially closer to the surface and the results clearly indicate that the SIMC-PID cannot tolerate $\theta = 2$ at these operating conditions unless variations up to $\pm$ 0.3 m can be allowed. It should also be noted that the AUV's velocities in surge and heave at lower depths are constantly large which in practice will make it impossible for operations, such as visual inspection using cameras, where a stable position is demanded.
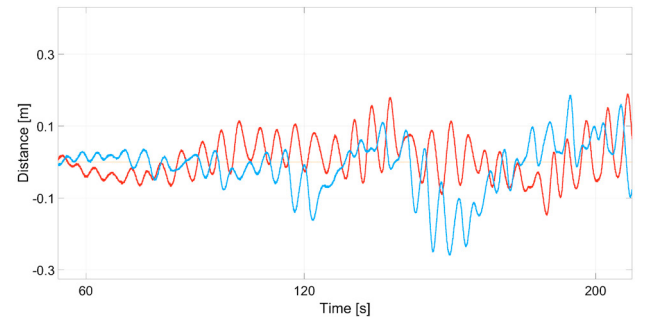

Fig. 4. For $\theta = 2$. The N (red) and E (blue) measured values where the references are 0, but the AUV is heaving step-wise.

Tab. 6. The mean oscillation amplitude for u and v at different depths. At each entry, the first value is for $\theta = 0.2$ and the second for $\theta = 2$.

Depth	Mean oscillation, u	Mean oscillation, v
25 m	±0.01 ; ±0.02 m	±0.01 ; ±0.03 m
20 m	±0.02 ; ±0.05 m	±0.03 ; ±0.05 m
15 m	±0.06 ; ±0.10 m	±0.06 ; ±0.11 m
10 m	±0.11 ; ±0.13 m	±0.08 ; ±0.13 m
5 m	±0.16 ; ±0.23 m	±0.17 ; ±0.25 m

7. CONCLUSION

This paper examines the performance of SIMC-PID for AUVs with output time delays and input disturbances. SIMC-PID is selected due to the simple tuning principle where time delays are explicitly included in the controller coefficients. Existing sensor technologies are evaluated and typical sensors (DVL and SBL) are used where dominant time delays exist in the N and E directions. The input disturbances are modeled as offshore waves and ocean currents where existing data from the North Sea is applied.

Simulations show that the D (depth) controller tolerates the time delay acceptably up to around 8 meters depth, while the roll, pitch, and yaw all perform acceptably in the entire range. When using the SIMC-PID controller, especially for the surge and sway motions, the DVL works acceptably up to around 7 to 8 meters depth, while the SBL introduces a time delay to these motions which cannot be above 15 m depth. It should be noted that a DVL in reality also introduces drifting in the signal and that has been neglected in this study.

It is concluded that the SIMC-PID controllers work well for most motions and at relatively small time delays. With larger time delays, such as being introduced by an SBL, more advanced controller schemes must be considered.

REFERENCES

Avila, J.P.J. and Adamowski, J.C. (2011). Experimental evaluation of the hydrodynamic coefficients of a rov through morison's equation. *Ocean engineering*, 38(17), 2162–2170. doi:10.1016/j.oceaneng.2011.09.032. URL `http://dx.doi.org/10.1016/j.oceaneng.2011.09.032`.

Benzon, M.v., Sørensen, F., Liniger, J., Pedersen, S., Klemmensen, S., and Schmidt, K. (2021). Integral sliding mode control for a marine growth removing rov with water jet disturbance. *2021 European Control Conference (ECC), IEEE Access*, 2265–2270. doi:10.23919/ECC54610.2021.9655050.

Benzon, M.v., Sørensen, F.F., Liniger, J., and Pedersen, S. (2022). Investigation of operating range of marine growth removing rov under offshore disturbances. *IFAC-PapersOnLine*. 14th IFAC Conference on Control Applications in Marine Systems, Robotics, and Vehicles CAMS 2022.

Brun, L. (2012). Rov/auv trends: market and technology. *Marine Technology Reporter*, 5(7), 48–51.

DNV (Det Norske Veritas) (2021). Environmental conditions and environmental loads. URL `https://www.dnv.com/oilgas/download/dnv-rp-c205-environmental-conditions-and-environmental-loads.html`.

Fossen, T.I. (2011). *Handbook of Marine Craft Hydrodynamics and Motion Control*. Wiley, Hoboken, 1. aufl. edition.

Hasselmann, K. (1973). *Measurements of wind-wave-growth and swell decay during the joint North Sea wave project*, volume 12. Deutsches Hydrographisches Inst, Hamburg.

Karmozdi, A., Hashemi, M., and Salarieh, H. (2018). Design and practical implementation of kinematic constraints in inertial navigation system-doppler velocity log (ins-dvl)-based navigation. *Navigation (Washington)*, 65(4), 629–642. doi:10.1002/navi.271. URL `https://onlinelibrary.wiley.com/doi/abs/10.1002/navi.271`.

Kebkal, K.G. and Mashoshin, A.I. (2017). Auv acoustic positioning methods. doi:10.1134/s2075108717010059.

Liniger, J., Jensen, A.L., Pedersen, S., Sørensen, H., and Mai, C. (2022). On the Autonomous Inspection and Classification of Marine Growth on Subsea Structures. In *Proceedings of the IEEE OCEANS 2022 conference*, 1–6. Chennai.

Mai, C., Pedersen, S., Hansen, L., Jepsen, K.L., and Yang, Z. (2016). Subsea infrastructure inspection: A review study. In *2016 IEEE International Conference on Underwater System Technology: Theory and Applications (USYS)*, 71–76. doi:10.1109/USYS.2016.7893928.

Manum, H. (2005). Extensions of Skogestad's SIMC tuning rules to oscillatory and unstable processes. 51–56. URL `https://folk.ntnu.no/skoge/diplom/prosjekt05/manum/rapport.pdf`.

Paull, L., Saeedi, S., Seto, M., and Li, H. (2014). Auv navigation and localization: A review. *IEEE Journal of Oceanic Engineering*, 39(1), 131–149. doi:10.1109/JOE.2013.2278891. URL `https://ieeexplore.ieee.org/document/6678293`.

Pedersen, S., Liniger, J., Sorensen, F.F., and von Benzon, M. (2022). On Marine Growth Removal on Offshore Structures. In *Proceedings of the IEEE OCEANS 2022 conference*, 1–5. Chennai.

Pedersen, S., Liniger, J., Sørensen, F.F., Schmidt, K., von Benzon, M., and Klemmensen, S.S. (2019). Stabilization of a rov in three-dimensional space using an underwater acoustic positioning system. volume 52, 117–122. doi:10.1016/j.ifacol.2019.11.037.

Sayer, P. (2008). Hydrodynamic loads during the deployment of rovs. *Ocean Engineering*, 35(1), 41–46. doi:10.1016/j.oceaneng.2007.07.005. URL `http://dx.doi.org/10.1016/j.oceaneng.2007.07.005`.

Skogestad, S. (2003). Simple analytic rules for model reduction and pid controller tuning. *Journal of Process Control*, 13(4), 291–309. doi:https://doi.org/10.1016/S0959-1524(02)00062-8. URL `https://www.sciencedirect.com/science/article/pii/S0959152402000628`.

Skogestad, S. (2006). Tuning for smooth pid control with acceptable disturbance rejection. *Industrial & Engineering Chemistry Research*, 45(23), 7817–7822. doi:10.1021/ie0602815. URL `https://doi.org/10.1021/ie0602815`.

Skogestad, S. and Grimholt, C. (2012). The simc method for smooth pid controller tuning.

Snyder, J. (2010). Doppler velocity log (dvl) navigation for observation-class rovs. 1–9. IEEE, Seattle, WA, USA. doi:10.1109/OCEANS.2010.5664561. URL `https://ieeexplore.ieee.org/document/5664561`.

Tena, I. (2011). Automating rov operations in aid of the oil & gas offshore industry. *SeeByte Whitepaper*, 1–9.

Vickery, K. (1998). Acoustic positioning systems. a practical overview of current systems. 5–17. IEEE. doi:10.1109/AUV.1998.744434. URL `https://ieeexplore.ieee.org/document/744434`.

Yang, Y. and Huang, G. (2017). Acoustic-inertial underwater navigation. *IEEE International Conference on Robotics and Automation (ICRA), Singapore*, 4927–4933.